Long term monitoring of the optical background in the Capo Passero deep-sea site with the NEMO tower prototype

104 AUTHORS, INCLUDING:

Bachir Bouhadef
INFN - Istituto Nazionale di Fisica Nucleare
36 PUBLICATIONS **225** CITATIONS

SEE PROFILE

Giacomo Cuttone
INFN - Istituto Nazionale di Fisica Nucleare
278 PUBLICATIONS **2,719** CITATIONS

SEE PROFILE

Valentina Giordano
INFN - Istituto Nazionale di Fisica Nucleare
102 PUBLICATIONS **983** CITATIONS

SEE PROFILE

Giuseppina Larosa
INFN- Istituto Nazionale di Fisica Nucleare, …
80 PUBLICATIONS **429** CITATIONS

SEE PROFILE

arXiv:1507.05024v1 [physics.ins-det] 17 Jul 2015

Long term monitoring of the optical background in the Capo Passero deep-sea site with the NEMO tower prototype

S. Adrián-Martínez[20], S. Aiello[4], F. Ameli[9], M. Anghinolfi[6], M. Ardid[20], G. Barbarino[7,15],
E. Barbarito[1,11], F.C.T. Barbato[7,15], N. Beverini[8,16], S. Biagi[3], A. Biagioni[9], B. Bouhadef[8],
C. Bozza[10,18], G. Cacopardo[3], M. Calamai[8,16], C. Calì[3], D. Calvo[21], A. Capone[9,17],
F. Caruso[3], A. Ceres[1], T. Chiarusi[2], M. Circella[1], R. Cocimano[3], R. Coniglione[3],
M. Costa[3], G. Cuttone[3], C. D'Amato[3], A. D'Amico[3,c], G. De Bonis[9], V. De Luca[3],
N. Deniskina[7], G. De Rosa[7,15], F. di Capua[7,15], C. Distefano[3], A. Enzenhöfer[22],
P. Fermani[9], G. Ferrara[3,13], V. Flaminio[8], L.A. Fusco[2,12], F. Garufi[7,15], V. Giordano[4],
A. Gmerk[3], R. Grasso[3], G. Grella[10,18], C. Hugon[6], M. Imbesi[3], V. Kulikovskiy[3],
R. Lahmann[22], G. Larosa[3], D. Lattuada[3], K.P. Leismüller[3], E. Leonora[4], P. Litrico[3],
C. D. Llorens Alvarez[20], A. Lonardo[9], F. Longhitano[4], D. Lo Presti[4,13], E. Maccioni[8,16],
A. Margiotta[2,12], A. Marinelli[8,16], A. Martini[5], R. Masullo[9,17], P. Migliozzi[7], E. Migneco[3],
A. Miraglia[3], C.M. Mollo[7], M. Mongelli[1], M. Morganti[8,19], P. Musico[6], M. Musumeci[3],
C.A. Nicolau[9], A. Orlando[3], A. Orzelli[6], R. Papaleo[3], C. Pellegrino[2,12], M.G. Pellegriti[3,a],
C. Perrina[9,17], P. Piattelli[3,b], C. Pugliatti[4,13], S. Pulvirenti[3], F. Raffaelli[8], N. Randazzo[4],
D. Real[21], G. Riccobene[3], A. Rovelli[3], M. Saldaña[20], M. Sanguineti[6], P. Sapienza[3],
V. Sciacca[3], I. Sgura[1], F. Simeone[9], V. Sipala[4], F. Speziale[3], A. Spitaleri[3], M. Spurio[2,12],
S.M. Stellacci[10,18], M. Taiuti[6,14], G. Terreni[8,16], L. Trasatti[5], A. Trovato[3], C. Ventura[4],
P. Vicini[9], S. Viola[3], D. Vivolo[7,15]

[1]INFN Sezione Bari, Via E. Orabona 4, 70126, Bari, Italy
[2]INFN Sezione Bologna, V.le Berti Pichat 6/2, 40127, Bologna, Italy
[3]INFN Laboratori Nazionali del Sud, Via S.Sofia 62, 95123, Catania, Italy
[4]INFN Sezione Catania, Via S. Sofia 64, 95123, Catania, Italy
[5]INFN Laboratori Nazionali di Frascati, Via Enrico Fermi 40, 00044, Frascati
[6]INFN Sezione Genova, Via Dodecaneso 33, 16146, Genova, Italy
[7]IINFN Sezione Napoli, Via Cintia, 80126, Napoli, Italy
[8]INFN Sezione Pisa, Polo Fibonacci, Largo Bruno Pontecorvo 3, 56127, Pisa, Italy
[9]INFN Sezione Roma, P.le A. Moro 2, 00185, Roma, Italy
[10]INFN Gruppo Collegato di Salerno, Via Giovanni Paolo II 132, 84084 Fisciano, Italy
[11]Dipartimento Interateneo di Fisica Università di Bari, Via E. Orabona 4, 70126, Bari, Italy
[12]Dipartimento di Fisica ed Astronomia Università di Bologna, V.le Berti Pichat 6/2, 40127, Bologna, Italy
[13]Dipartimento di Fisica e Astronomia Università di Catania, Via S. Sofia 64, 95123, Catania, Italy
[14]Dipartimento di Fisica Università di Genova, Via Dodecaneso 33, 16146, Genova, Italy
[15]Dipartimento di Scienze Fisiche Università di Napoli, Via Cintia, 80126, Napoli, Italy
[16]Dipartimento di Fisica Università di Pisa, Polo Fibonacci, Largo Bruno Pontecorvo 3, 56127, Pisa, Italy
[17]Dipartimento di Fisica Università "Sapienza", P.le A. Moro 2, 00185, Roma, Italy
[18]Dipartimento di Fisica Università di Salerno, Via Giovanni Paolo II 132, 84084 Fisciano, Italy
[19]Accademia Navale di Livorno, viale Italia 72, 57100 Livorno, Italy
[20]Instituto de Investigación para la Gestión Integrada de las Zonas Costeras, Universitat Politècnica de València, Gandia, Spain
[21]IFIC-Instituto de Física Corpuscular, (CSIC-Universitat de València), València, Spain
[22]Erlangen Centre for Astroparticle Physics, Friedrich-Alexander-Universität Erlangen-Nürnberg,Erlangen, Germany

Abstract The NEMO Phase-2 tower is the first detector which was operated underwater for more than one year at the "record" depth of 3500 m. It was designed and built within the frame-

[a]e-mail: pellegriti@lns.infn.it
[b]e-mail: piattelli@lns.infn.it
[c]Present address: Nikhef, Science Park, Amsterdam, The Netherlands

work of the NEMO (NEutrino Mediterranean Observatory) project. The 380 m high tower was successfully installed in March 2013 80 km offshore Capo Passero (Italy). This is the first prototype operated on the site where the italian node of the KM3NeT neutrino telescope will be built. The installation and operation of the NEMO Phase-2 tower has proven

the functionality of the infrastructure and the operability at 3500 m depth. A more than one year long monitoring of the deep water characteristics of the site has been also provided. In this paper the infrastructure and the tower structure and instrumentation are described. The results of long term optical background measurements are presented. The rates show stable and low baseline values, compatible with the contribution of ^{40}K light emission, with a small percentage of light bursts due to bioluminescence. All these features confirm the stability and good optical properties of the site.

1 Introduction

High energy neutrinos are expected to be messengers from astrophysical objects where hadronic interactions may take place. In this framework several projects were developed (see refs. [1–3]). The recent discovery of a cosmic neutrino flux reported by IceCube [4] initiated the era of neutrino astronomy confirming that a detector with size of the order of several km^3 is required for high energy ($E \geq$ TeV) neutrino investigation. However, most of the questions raised about the origin of the observed neutrino cosmic flux remain unsolved. Many hypotheses have been proposed including galactic and extragalactic sources, Dark Matter etc. As a consequence of this discovery, the physics case for the construction of a km^3-scale neutrino telescope in the Northern Hemisphere is strongly enforced. A telescope in the Mediterranean Sea has an optimal field of view of the Galactic Plane due to the Earth rotation. Moreover, the better angular resolution achievable with respect to IceCube, due to the large effective scattering length in deep sea water ($\geq$ 200 m), enhances the pointing accuracy increasing the possibility of neutrino source identification.

Since 1998, the NEMO (NEutrino Mediterranean Observatory) collaboration carried out research activities aimed at developing and validating key technologies for a km^3-scale underwater neutrino telescope [5–8] as well as searching and characterizing a deep-sea site suitable for the installation of the detector. The first pilot project, NEMO Phase-1, dates back to 2007 when a prototype tower was deployed at a depth of 2000 m in a Test Site located about 20 km offshore Catania (Italy). Technical details and the scientific results can be found in [9].

A deep-sea site, located at a depth of 3500 m about 80 km offshore Portopalo di Capo Passero (Italy) (36° 17′ 48″ N, 15° 58′ 42″ E), was identified as optimal for the installation of the underwater neutrino telescope (Fig 1). In the following it is indicated as the KM3NeT-It site.

In 2008 a 100 km electro-optical cable connecting the KM3NeT-It site to an on-shore station, located in Portopalo di Capo Passero, was deployed. In the following years an important R&D activity aimed at validating new technologies was carried out thanks to this infrastructure. These activities culminated in the construction, deployment and operation of the NEMO Phase-2 tower in March 2013. The Phase-2 tower continuously took data until August 2014 when it was disconnected to allow for an upgrade of the underwater infrastructure in preparation for the installation of the first group of detection structures that will form the italian node of the KM3NeT detector.

The paper is structured as follows. In Section 2 the Capo Passero site and infrastructure are described. Section 3 describes the detection tower and the details of all the included sub-systems. Section 4 describes the installation and the sea operations, which are necessary for the long-term measurements of the optical background presented in Section 5. Conclusion and perspectives are given in Section 6.

2 The KM3NeT-It site and infrastructure

The KM3NeT-It site was characterised with a series of sea campaigns to study and monitor the most important environmental parameters. Oceanographical properties of the site, like deep-sea water optical properties (absorption and diffusion), water environmental properties (temperature, salinity), biological activity, optical background, water currents, sedimentation and seabed nature were studied [10–12]. This activity has confirmed that the KM3NeT-It site has optimal characteristics to host the italian node of the KM3NeT research infrastructure [13].

The KM3NeT-It infrastructure includes a shore station, a 100 km long main electro-optical cable (MEOC) and a deep-sea installation comprising a novel design 10 kW DC voltage converter. The onshore infrastructure, located in Portopalo di Capo Passero, hosts the power feeding system, which directly feeds the MEOC [14], as well as the control centre and the data acquisition system.

The MEOC is a standard submarine communication cable manufactured by Alcatel[1] containing 20 G655 optical fibres[2]. These fibres have a maximum attenuation of 0.23 dB/km at 1550 nm wavelenght. The cable has a single conductor for power transmission. Current return is provided via seawater, which offers an extremely small resistance thus reducing power losses [15]. The system incorporates sea electrodes both at the shore (anode) and at the deep-sea (cathode) ends. At the deep-sea end the MEOC is terminated by a Cable Termination Frame (CTF) (Figs. 2,3) hosting a Cable Termination Assembly (CTA), allowing to split and reroute the fibres towards a connection panel, and a DC Medium Voltage Converter (MVC) to step down the 10 kV provided by the onshore Power Feeding System to 375 V [16]. The intermediate voltage is distributed to three output ports equipped

---

[1]Model OALC-4 17 mm Type 30.
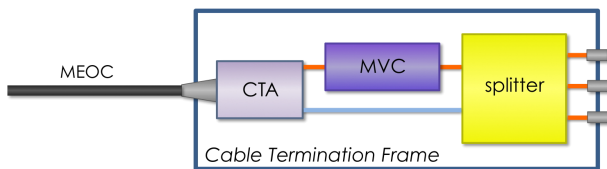[2]Corning Vascade LEAF negative dispersion NZ-DSF.

Fig. 2 Scheme of the Cable Termination Frame. Power lines and optical fibres of the Main Electro Optical Cable (MEOC) are split by a Cable Termination Assembly (CTA). The 10 kW DC/DC Medium Voltage Converter (MVC) steps down the voltage from 10 kV to 375 V. A splitter assembly reroutes power lines and optical fibres towards three wet-mateable electro-optical connectors.

with wet-mateable connectors. Similarly optical fibre communication is distributed to the same output ports. Connections are performed by means of a Remotely Operated Vehicle (ROV). In this configuration eight out of the twenty optical fibres of the MEOC are unfolded and distributed to the three outputs. The construction and installation of a new CTF using all the twenty available fibres is under way.

3 The NEMO Phase-2 tower

The detection unit deployed in the KM3NeT-It site at a depth of 3449 m is a tower-like structure composed of eight horizontal elements (named *floors*). Each floor is a 8 m long marine grade aluminum structure connected to its next neighbours by means of eight tensioning ropes [17]. The arrangement of these ropes is such that each floor is forced to a position perpendicular to its vertical neighbours, as shown in Fig. 4. An iron anchor fixes the structure to the seabed while an appropriate buoyancy at the top provides the pull
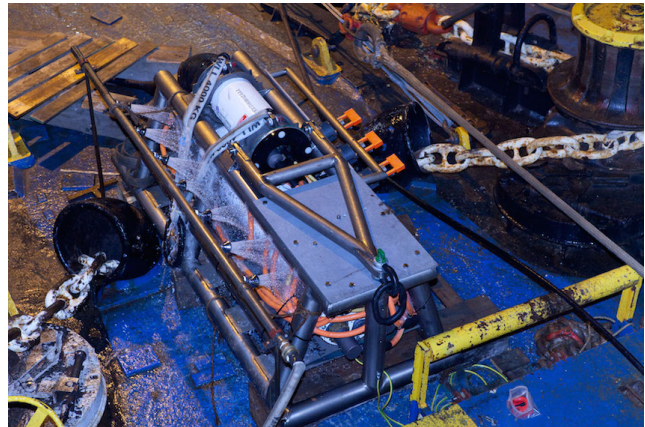

Fig. 3 An image of Cable Termination Frame on the ship deck prior to its deployment.

to keep the structure taut. The floors are vertically spaced by 40 m, with the lowermost one positioned 100 m above the sea bottom. Each floor holds four Optical Modules (OM), two at each end, one looking vertically downwards and the other horizontally outwards. The structure is designed to be assembled and deployed in a compact configuration (Fig. 5) and to be unfurled once on the sea bottom under the pull provided by the buoy.

A schematics of the tower is shown in Fig. 6. In addition to the 32 OMs the instrumentation installed includes several sensors for calibration and environmental monitoring. In particular for positioning calibration purposes two hydrophones are installed close to the ends of each floor and two others on the tower base. Being the deep seawater a dynamical medium, monitoring of its oceanographic and optical properties during the detector operation is important since they can have an impact on the detector performance. For that reason environmental probes are installed on the tower: two Conductivity–Temperature–Depth (CTD) probes [3], installed on the 1st and 7th floor; a light transmissometre used for the measurement of blue light attenuation in seawater (C*); a Doppler Current Sensor (DCS) used to monitor deep sea currents installed on the 5th floor.

Power distribution and data transmission along the tower is fulfilled by means of a "backbone" electro-optical cable. This is a lightweight umbilical subsea cable[4], carrying 10 electrical conductors and 12 optical fibres.

3.1 The Optical Modules

The OM is the basic element of the NEMO Phase-2 detection unit [18, 19]. Each OM consists of a 13-inch pressure resistant (up to 700 bar) borosilicate glass sphere[5], housing

---

[3]Sea Bird Electronics, 37-SM Micro-CAT.
[4]Nexans S.A.
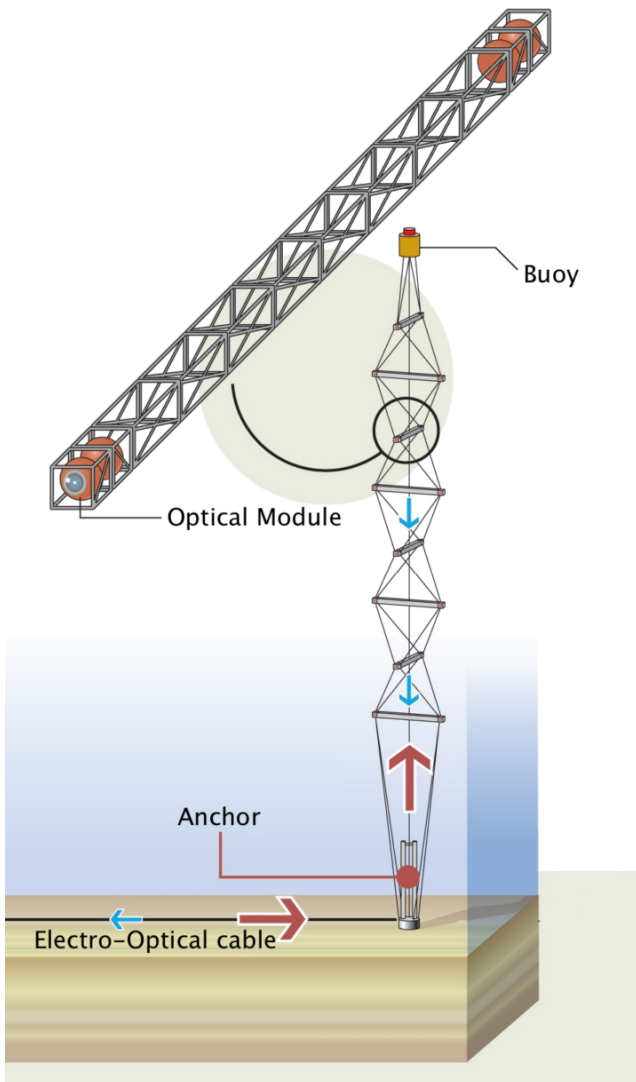[5]Nautilus Marine GmbH, VITROVEX flotation sphere.

Fig. 4 Sketch of the NEMO Phase-2 tower. The structure is formed by a sequence of eight floors, each one supporting four optical modules. The structure is anchored at the seabed and kept taut by a buoy located at the top. Vertical distances are not to scale.

Fig. 5 The NEMO Phase-2 tower in its compact configuration during the integration phase.
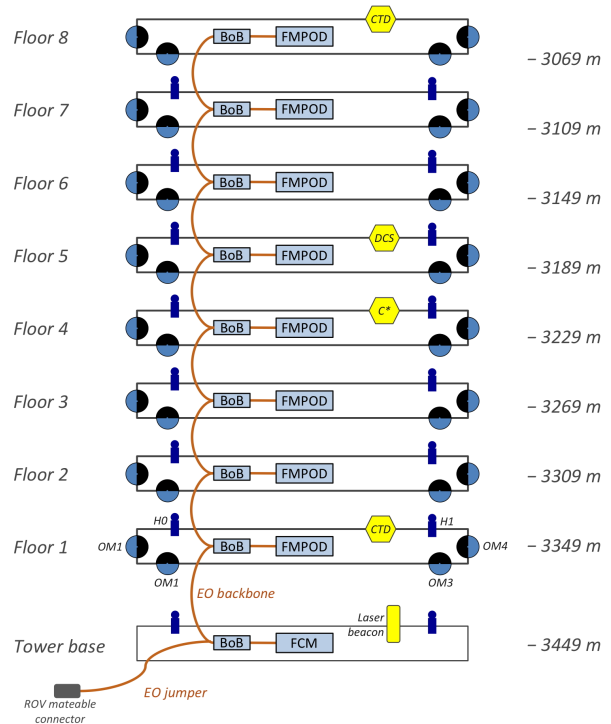

Fig. 6 Schematics of the NEMO Phase-2 tower, including the backbone cabling (orange), the Floor Module Protective Oceanic Device (FMPOD) and the electro-optical breakouts (BoB). Connection to the Junction Box is provided through a ROV-mateable hybrid connector, installed in the tower base. The position of the environmental probes are also indicated as well as those of the hydrophones (H0 and H1) (see text for details). Nominal depths of each floor are given on the right.
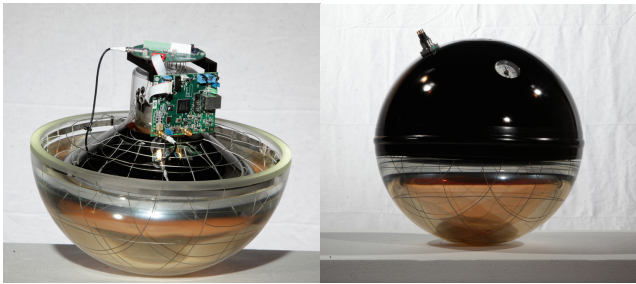
a 10-inch Hamamatsu photomultiplier (PMT R7081-SEL) [20] together with its high-voltage power supply, read-out electronics and calibration system (Fig. 7). Mechanical and optical contact between the PMT and the internal glass surface is ensured by an optical silicone gel. A μ-metal cage shields the PMT from the Earth's magnetic field. A detailed description is given in [18].

PMT signal digitization is provided by a Front-End Module board that is also housed inside the OM [21]. The board samples the analog PMT signal using two 8-bit Fast Analog to Digital Converters (Fast-ADCs) running at 100 MHz and staggered by 5 ns. This technique gives the desired sampling rate yet allowing for a power dissipation lower than a single 200 MHz ADC. To match the large dynamic range of

Fig. 7 Left: One hemisphere of the optical module glass vessel containing the photomultiplier and the front-end module board. Right: An optical module fully integrated with the electro-optical feedthrough and the pressure-meter.

Fig. 8 Schematics of the floor system. See text for the definition of the acronyms.

the PMT signal to the input voltage range of the ADCs, the signal is compressed by a non-linear circuit, which applies a quasi-logarithmic signal compression.

Four OMs were also equipped with a prototype RFID based system that allowed to acquire oceanographic data with readout through the glass sphere without the use of feedthroughs [22].

3.2 Electronics and Cabling

A simplified scheme of the electronics and cabling of the tower is shown in Fig. 8. At the level of each floor the backbone is split by means of breakout boxes (BoB). Each breakout is a high-density polyethylene vessel filled with silicone oil and pressure compensated. The BoB is equipped with two hybrid penetrators, which are used to split the backbone, and two connectors (one electrical and one optical) from the backbone to the floor cabling system.

On each floor the four OM digital data are sent to a Floor Control Module board (FCM) housed in a pressure resistant vessel, the Floor Module Protective Oceanic Device (FM-POD). The FMPOD is fitted in the middle of the floor mechanical structure and houses the data acquisition, control and the power distribution systems of the floor. A similar setup is adopted for the tower base.

The 375 V supplied by the MVC is monitored at the level of the tower base and distributed to the eight floors. Inside the floor FMPOD a Power Contol System board (PCS) provides conversion of the DC supply from 375 V to the low voltages needed by the electronics as well as monitoring and control of the main electrical parameters of the floor.

A Slow Control Interface board (SCI) provides the interface to the oceanographic instruments installed on the floor via RS-232 serial standard. In addition, each SCI has two analogue sensors to monitor humidity and temperature inside the FMPOD.

The acoustic board (AcuBoard) is a part of the positioning system described in section 3.5.1.
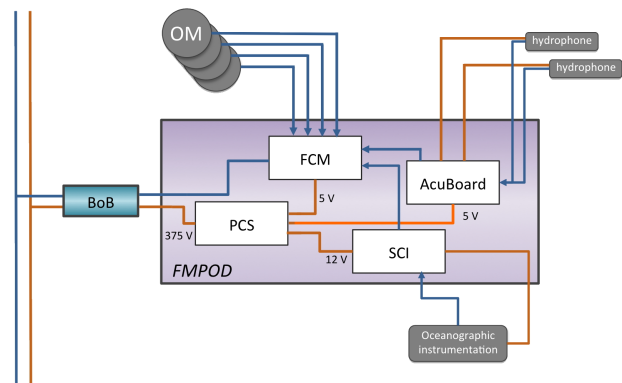
3.3 Data Transmission System

The link to the shore-station uses an optical fibre as physical layer and implements a high speed serial link using a proprietary data format [23]. All data are encoded into a serial 800 Mb/s stream by a serializer, converted into optical signal by an electro-optical transceiver and transmitted to the shore station. In the communication protocol the data stream is divided into 125 μs long frames of 10000 bytes each.

A transmission system through optical links based on Dense Wavelength Division Multiplexing (DWDM) technology was chosen [24]. It is implemented by means of *add-and-drop* passive devices that multiplex/demultiplex many optical channels at different wavelengths into/from the same fibre. Two wavelengths are associated to each floor of the tower, one for the sea-to-shore and one for the shore-to-sea communication. The optical wavelengths are chosen according to the ITU standard grid with 100 GHz frequency spacing in the C-Band thus allowing up to 45 channels per fibre. The DWDM network provides, indeed, a *point-to-point* communication between the shore-station equipment and the deep-sea apparatus. Each FCM contains an add-and-drop filter that allows to add or subtract the specific optical wavelength allocated to the floor. Data from all floors are thus transmitted through the backbone in the same fibre.

Detector data are received onshore by a dedicated electronics board, named Ethernet FCM (EFCM), which is based on a Virtex-5[6] development board. This board collects the data received by the underwater electronics and transfers them to the DAQ and storage systems through a Gigabit Ethernet connection.

---

[6]Xilinx Inc.

3.4 Data Acquisition System

Thanks to the extremely large communication bandwidth available (2 Gpbs), no hardware triggers are implemented underwater: all the digitized signals are sent to shore. The data stream originated by each FCM is addressed on shore to the twin EFCM board, which transfers the data to the on-shore Trigger and Data Acquisition System (TriDAS) [25].

Each detected photon pulse is sampled by the FEM and arranged by the FCM in a hit record with a mean size of 28 bytes. Consequently the tower averaged optical throughput is about 250 Mbps. The total amount of data from offshore includes also a stream of about 80 Mbps from the acoustic sensors and a negligible contribution of slow control data. The electronics were designed to deal with an optical signal up to 150 kHz continuous single rate on each PMT without dead time.

From the EFCMs, the PMT optical data-stream is routed through a 1 Gb Ethernet network to the first layer of the TriDAS, composed of two Hit Managers (HM) processes running on two CPUs. Each HM gathers data from half a tower and coherently time-slices the continuous stream of data into time intervals of 200 ms. All the data corresponding to a given interval of time are sent by the HMs to a single TriggerCPU process (TCPU). Subsequent time slices are addressed to the others TCPU processes, implementing the trigger algorithms for background rejection. A reduced selected stream is then addressed, through a 1 Gb Ethernet switch, from all the TCPUs to the Event Manager (EM) server which is deputed to write the trigger selected data on the local temporary storage device. Finally data are copied to the long lasting storage facility at the Laboratori Nazionali del Sud in Catania (Italy) by means of a dedicated 1 Gb Ethernet point to point connection.

3.5 Positioning and calibration

3.5.1 Acoustic positioning system

Since the tower structure is not rigid, floors are subject to the effects of deep-sea currents than can distort the vertical line shape of the tower, making the floors rotate and tilt. For a proper reconstruction of the muon tracks, which is based on space-time correlation of Cherenkov photons hitting the OMs, the knowledge of the position of each OM with a precision of the order of 10 cm is needed. This can be obtained by using a system based on acoustic triangulation as demonstrated by previous experience gained with the NEMO Phase-1 prototype [9].

The acoustic positioning system installed on the NEMO Phase-2 tower consists of couples of hydrophones mounted in fixed positions close to the end of each floor (H0 and H1

in Fig. 6) [26, 27]. For testing and validation purposes different types of hydrophones were used. The six lowermost floors are equipped with large broadband hydrophones (10 Hz - 70 kHz)[7]. A couple of free flooded rings (FFR) hydrophones[8] is installed on the 7th floor. Finally, two of the OMs on the 8th floor are equipped with custom designed piezoelectric acoustic sensors glued to the internal surface of the glass sphere. Data from all acoustic receivers are sampled offshore at a frequency of 192 kHz with a 24 bit resolution and continuously sent to shore. Offshore data are time stamped with the absolute acquisition time by a dedicated synchronous system which is phased with a GPS time station[9]. The acoustic position system is completed with a set of autonomous acoustic beacons installed on the seafloor at a distance of approximately 400 m from the tower and one beacon at the base of the tower.

An independent real time monitoring of the floor orientation is provided by an Attitude Heading Reference System (AHRS), that includes triaxial gyroscopes, accelerometers and magnetometers, placed inside each FMPOD.

3.5.2 Time calibration System

The reconstruction of physical events (e.g., muon tracks) requires sub-nanosecond synchronisation between the OMs.

The synchronous communication protocol implemented on the tower provides synchronization with a unique clock source (Master Clock) for all electronics boards and OMs. The clock distribution system is based on a GPS station, which provides the absolute time, encoded in IRIG-B 100-1344 standard, and a high-stability 10 MHz clock which works as Master Clock for the detector [28].

Due to the clock propagation delay from shore to the tower, each OM has its own time offset to be measured and compensated. This is done using a fast light pulser installed in each OM. The light pulsers are controlled by dedicated FPGA[10] based control boards located in each FMPOD, which also allow setting the intensity and the frequency of the flashes of each light pulser. The system is operated from shore. The control boards can also perform measurements of the propagation delays of the commands to reach each of the light pulsers. The propagation delays have been proven to remain stable down to the level of the resolution of the measurements, i.e. within 100 ps.

Prior to the deployment, a calibration of the OMs of the full tower has been performed by using an external system exploiting a fast laser source (Hamamatsu PLP-10) coupled to a network of optical fibres of calibrated lengths. Multi-

---

[7]Model SMID TR-401.
[8]Sensor Technology Ltd.
[9]Symmetricom XLi.
[10]Altera Cyclone III.

mode, graded index optical fibres have been used for this application.

In order to have redundancy in time calibration, for exploring new solutions proposed for a km^3-size detector as well as for measurements of the optical properties of water, the NEMO Phase-2 tower is also equipped with additional calibration devices comprising small LED pulsers, installed inside selected OMs in such a way to illuminate the OMs of the upper floors, and a laser beacon installed on the base of the tower.

4 Installation and operation

The NEMO Phase-2 tower was deployed on March 23 2013 during a sea campaign operated by the Multi Service Vessel 'Nautical Tide'[11]. The tower deployment operations took approximately 6 hours. The tower was first lowered to the seabed and then connected to the CTF by means of a surface controlled ROV. After the connection the tower was unfurled reaching its final configuration. Data acquisition started immediately.

During the same operation one autonomous acoustic beacon was also deployed at about 400 m North of the tower. A second one was installed in a separate sea campaign on July 20 2013 at about 400 m East of the tower. Together with the one installed on the tower base they form the acoustic Long Baseline (LBL) system. These beacons were not synchronized to the GPS clock distributed from shore. Their time of emission had to be re-synchronised with respect to the detector clock by means of the monitoring hydrophone mounted on the tower base in a fixed and known position. After the deployment the power line to the monitoring hydrophones did not behave properly, thus preventing the possibility of calibrating the LBL system. Consequently it was not possible to determine the position of each single hydrophone of the tower. However, information on the vertical position of the tower was provided by the CTD probes which were found to be at the expected mean depths of 3358 m (1st floor) and 3118 m (7th floor). This information was checked by measuring the time delays of acoustic signals, emitted by the beacon installed on the tower base, between the 1st floor and the other floors and found to be consistent with the CTD data.

Although in a reduced configuration, the acoustic data allow to recover the orientation (heading) and pitch and roll of each floor with a precision better than 1 degree. Using a global fit algorithm, the position of each hydrophone was calculated with an estimated error of about 1 m. The acoustic data were combined with depth information from the two CTDs. A fixed distance between floors of 40 m and a 5 m uncertainty on the position of the LBL beacons, determined
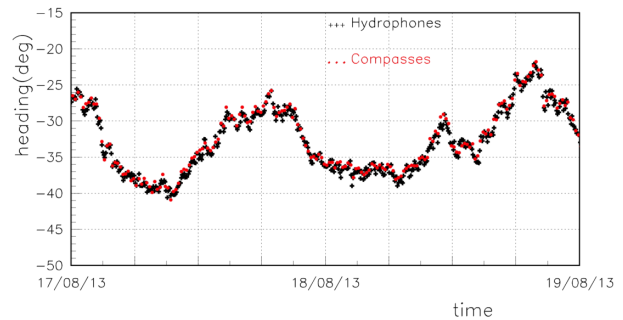
Fig. 9 Orientation of Floor 6 determined using the hydrophone data (black crosses) compared to the heading information determined by the AHRS installed on the Floor Control Module.

by the ship GPS system at the time of deployment, were assumed. As an example, a floor heading reconstruction by using the hydrophones system is shown in Fig. 9 for period of two days. This is in excellent agreement with the AHRS heading reconstruction (15 minutes averages) normalized to the hydrophone data.

Despite the lack of a precise positioning of each single OM it was however possible to reconstruct downgoing muon tracks and determine the Depth Intensity Relation of muons in water as reported in [29].

In a limited number of runs a new test device, i.e. a beacon located at the tower base whose emission is synchronous with the master clock, was used. In this case it was possible to reduce the effect of systematic errors and determine the position of each hydrophone with an accuracy of about 30 cm comparable to those obtainable with a complete LBL.

The commissioning phase of the tower lasted up to 30 June 2013. During this phase the PMT gains were adjusted several times to obtain the same gain factor of 5×10^7. This converts each single photon electron (s.p.e.) into a mean integrated charge of about 8 pC. Thresholds were adjusted at approximately 0.25 single photo-electron (s.p.e.). As a consequence data rates reported in the following have to be considered stable only after the completion of this phase.

5 Long term monitoring of the optical background

During seventeen months of operation the NEMO Phase-2 tower allowed for a continuos long term monitoring of the site characteristics. In particular, the optical background rate, due to the presence of Cherenkov light produced in the decay of ^{40}K as well as light emitted by bioluminescent organisms, was studied.

The distribution of the time difference between successive hits, Δt, of a typical OM, is shown in Fig. 10. It has the expected exponential form, with a slope of $\tau = 1.8 \times 10^{-5}$
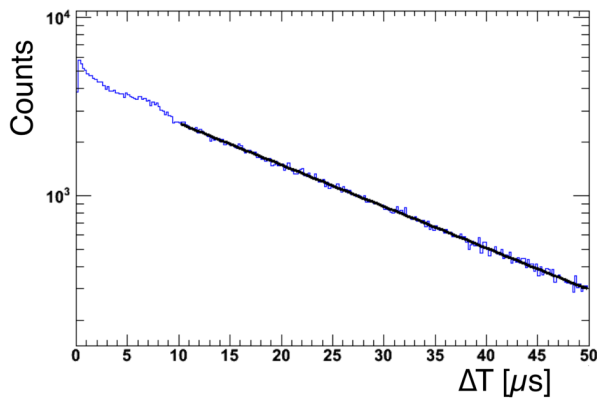
Fig. 10 Time difference between two consecutive hits. The exponential fit above $\Delta t = 10\mu s$ (black line) gives a characteristic time $\tau = 1.8 \times 10^{-5}$ s. The bump at $\Delta t \approx 7\mu s$ is due to the presence of PMT afterpulses. For $\Delta t < 1\mu s$ the effect of electronics deadtime is present.

s corresponding to a purely random background singles rate of about 55 kHz.

The expected singles rate has been evaluated by using a complete GEANT4 simulation, that accounts for the ^{40}K contribution, the PMT dark counts and the presence of radioactive materials in the glass sphere [30]. The latter two were measured in the laboratory. The water absorption length of the KM3NeT-It site has been used [11]. The result of this simulation gives a value of 54 ± 3 kHz in agreement with the in situ observed rate.

The rates determined as in Fig. 10 on the acquired data suffer of the dead time introduced by the data acquisition system that limits the maximum data rate transferable to about 150 kHz. However, the FEM board on each OM provides an independent monitoring of the average count rate by counting once per second the number of hits with amplitude exceeding a threshold of ≈ 0.25 single photo-electron (s.p.e.) in a 10 ms time window. This estimate does not suffer of dead time limitations allowing to monitor the signal rate up to about 6.5 MHz. Figure 11 shows the distribution of the singles rates (measured by the OM rate monitor) in one OM for two one-hour time slots taken in different periods with different optical background characteristics. In the top panels (a and b) the rate is shown as a function of time. In the bottom panels (c and d) the corresponding histograms of the rate distributions are shown. In general, the instantaneous rate exhibits a flat baseline at around 55 kHz with some sporadic bursts. The baseline corresponds to the contribution of the ^{40}K discussed above while light bursts can be attributed to the presence of bioluminescent organisms. The amount of these bursts can vary in time, as shown by the two examples in Fig. 11. To monitor these variations, as well as possible variations in the baseline rate, histograms like those of Figs. 11c)-d) have been built for 15 minutes long time
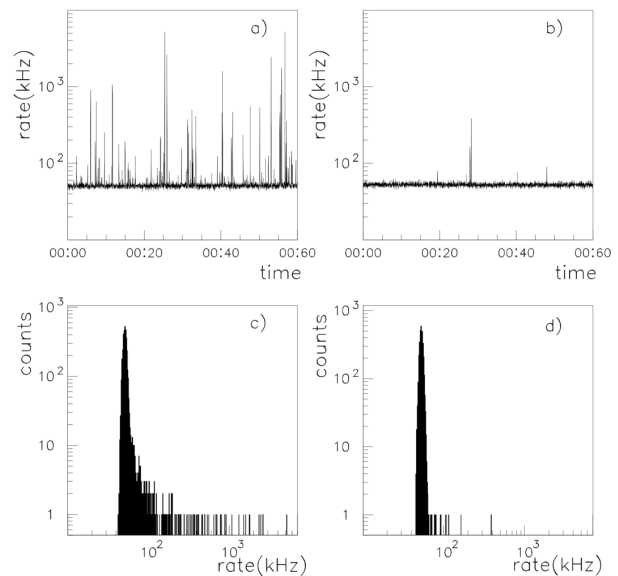

Fig. 11 Singles rate as measured in the monitoring channel as a function of time for one hour time slots measured on July 7 2013 (panel a) and on September 11 2013 (panel b). Panels c) and d) show the corresponding histograms of the monitored rate values.

frames covering the whole operation period. From each histogram the baseline rate was extracted with a Gaussian fit. The amount of light bursts was determined as the fraction of time with rate exceeding an arbitrarily fixed threshold of 100 kHz (burst fraction).

In Fig. 12, the baseline rate for eight OMs, all chosen with the same down-looking orientation and located at different depths, is shown for the whole operation period of the tower. For sake of completeness the data taken during the commissioning period are also shown (light blue dots). The observed baseline rates do not show large fluctuation above 50-60 kHz and are in agreement with previous measurements performed in the same site. The average value for the whole measurement period and for all floors is compatible with the estimate of the ^{40}K decay contribution. No significant effect due to the depth is observed.

For the same set of eight down-looking OMs the Probability Density Function of having a rate exceeding 100 kHz in a 10 ms time interval are reported in Fig. 13. No significant depth dependence is observed. This effect can be seen also in Fig. 14 (upper panel) where the Probability Density Function of the rate has been calculated after the last HV adjustment for the period going from July 2013 until August 2014. In particular, the contribution of bioluminescence bursts is shown for an optical module located on the 1st floor of the tower. For the examined PMT, the rate distribution is peaked around 50 kHz and becomes negligible above 100 kHz. The other optical modules show very similar behaviors with peaks located in the range 45-55 kHz. The Cumulative Density Function of the rate has also been calculated
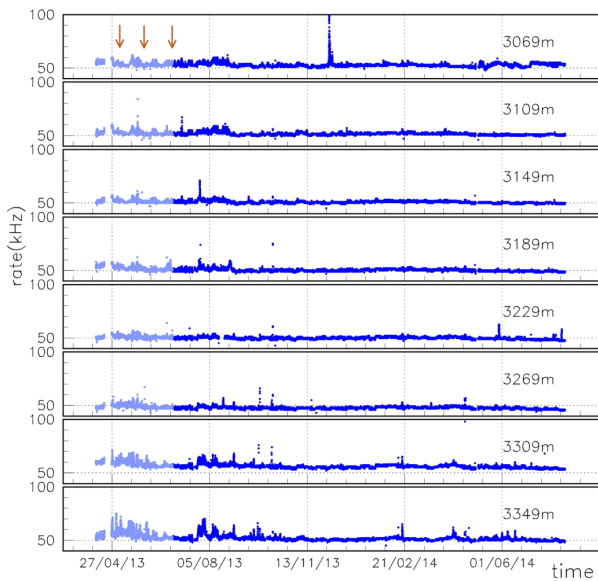
Fig. 12 Baseline rate measured for the whole operation period of the tower at different depths. All selected PMTs are down-looking. Light blue dots correspond to the commissioning period of the detector. The arrows indicate the dates when PMT high voltage adjustments were performed.
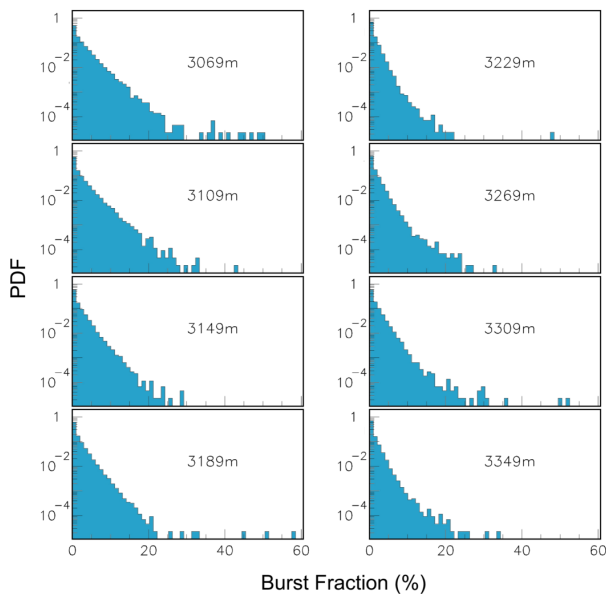

Fig. 14 Probability Density Function (PDF) and Cumulative Density Function (CDF) of singles rate (black dots) for the whole set of data taken from July 2013 to August 2014 of one PMT. The solid red line indicates the result of the GEANT4 simulation described in the text. Dashed red lines give the error in this simulation.

Fig. 13 Probability Density Function (PDF) of observing a given burst fraction, defined as having a rate exceeding 100 kHz in a 10 ms time window, in eight down-looking OMs placed at different depths.

Fig. 15 a) baseline rates over a 15 minutes period; b) burst fraction (b.f.), defined as the fraction of time in the 15 minute window with rate exceeding 100 kHz; c) modulus of the water current velocity measured with the DCS.

The time behaviour of the small bioluminescence activity is shown in Fig. 15 for a 15 days time series. There is evidence of periodic behaviour due to the presence of inertial currents which at the tower latitudes have a period of 20.21 h. Further analyses of bioluminescence correlation with sea currents are in progress.

6 Conclusions and perspectives

Deployed in March 2013 in the abyssal site of Capo Passero at the depth of 3500 m, the NEMO Phase 2 tower continuously took data until August 2014, validating the techni-

and it reaches the value of 0.99 in the range 100-200 kHz. This leads to the important conclusion that the probability to have the TriDAS in dead time is less than 1% all along the full year observation. There is no period in which the OMs needed to be switched off for high bioluminescence activity.
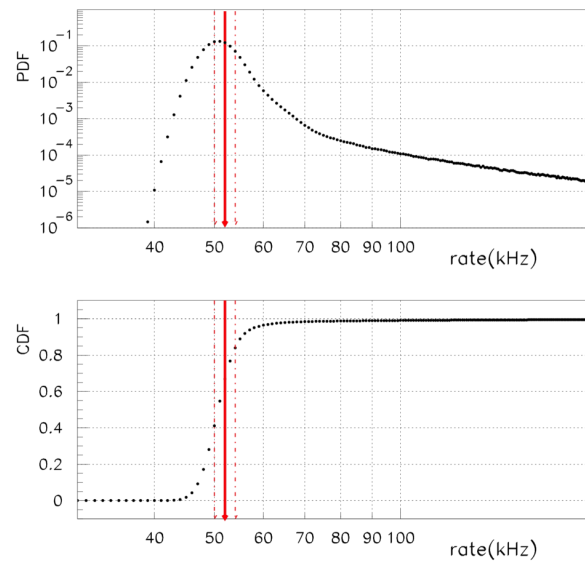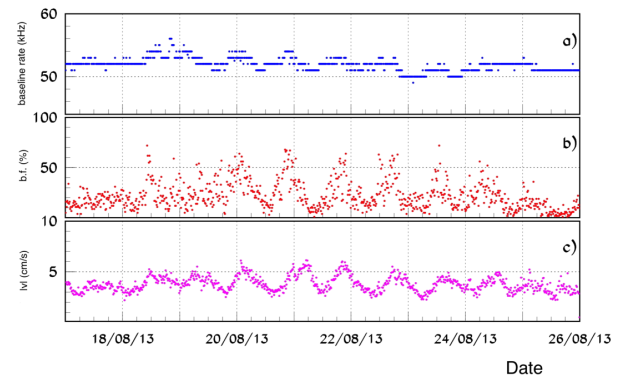
cal solutions proposed for the construction of an underwater Cherenkov neutrino detector. The data analyses have confirmed the optimal environmental characteristics of the site which, starting from 2015, will host the italian node of the KM3NeT underwater neutrino telescope.

References

1. M. Ageron et al., ANTARES: the first undersea neutrino telescope. Nucl. Instr. and Meth. A **656**, 11 (2011)

2. V. Aynutdnov for the Baikal Coll., The BAIKAL neutrino project: results and perspective. Nucl. Instr. and Meth. A **628**, 115 (2011)

3. A. Achterberg et al., First year performance of the IceCube neutrino telescope. Astropart. Phys. **26**, 155 (2006)

4. M.G. Aartsen et al., Evidence for high-energy extraterrestrial neutrinos at the IceCube detector. Science **342**, 1242856 (2013)

5. E. Migneco et al., Status of NEMO. Nucl. Instr. and Meth. A **567**, 444 (2006)

6. E. Migneco et al., Recent achievements of the NEMO project. Nucl. Instr. and Meth. A **588**, 111 (2008)

7. A. Capone et al., Recent results and perspectives od the NEMO project. Nucl. Instr. and Meth. A **602**, 47 (2009)

8. M. Taiuti et al., The NEMO project: A status report. Nucl. Instr. and Meth. A **626**, S25 (2011)

9. S. Aiello et al., Measurement of the atmospheric muon flux of the NEMO Phase-1 detector. Astropart. Phys. **33**, 263 (2010)

10. A. Capone et al., Measurements of light transmission in deep sea with the AC9 transmissometer. Nucl. Instr. and Meth. A **487**, 423 (2002)

11. G. Riccobene et al., Deep seawater inherent optical properties in the Southern Ionian Sea. Astropart. Phys. **27**, 1 (2007)

12. A. Rubino et al., Abyssal undular vortices in the Eastern Mediterranean basin. Nature Communications **3** 834 (2012)

13. KM3NeT web site: <www.km3net.org>

14. M. Sedita for the NEMO collaboration, Electro-optical cable and power feeding system for the NEMO Phase-2 project. Nucl. Instr. and Meth. A **567**, 531 (2006)

15. R. Cocimano for the NEMO collaboration, A comparison of AC and DC power feeding systems based on the NEMO experiences. Nucl. Instr. and Meth. A **602**, 171 (2009)

16. A. Orlando for the NEMO collaboration, On line monitoring of the power control and engineering parameters systems of the NEMO Phase-2 tower. Nucl. Instr. and Meth. A **602**, 180 (2009)

17. M. Musumeci for the NEMO coll., Construction and deployment issues for a km3 underwater detector. Nucl. Instr. and Meth. A **567**, 545 (2006)

18. S. Aiello et al., The Optical modules of the phase-2 of the NEMO project. JINST **8**, P07001 (2013)

19. E. Leonora and S. Aiello, Design and assembly of the optical modules for phase-2 of the NEMO project. Nucl. Instr. and Meth. A **725**, 234 (2013)

20. S. Aiello et al., Procedures and results of the measurements on large area photomultipliers for the NEMO project. Nucl. Instr. and Meth. A **614**, 206 (2010)

21. C.A. Nicolau for the NEMO collaboration, An FPGA-based readout electronics for neutrino telescopes. Nucl. Instr. and Meth. A **567**, 552 (2006)

22. M. Cordelli et al., PORFIDO: Oceanographic data for neutrino telescopes. Nucl. Instr. and Meth. A **626-627**, S109 (2011)

23. F. Ameli et al., The Data Acquisition and Transport Design for NEMO Phase-1. IEEE Trans. on Nucl. Sci. **55**, Issue 1 233 (2008)

24. A. D'Amico for the NEMO coll., Design of the optical Raman amplifier for the shore station of NEMO Phase-2. Nucl. Instr. and Meth. A **626-627**, S173 (2011)

25. T. Chiarusi for the NEMO coll., Scalable TriDAS for the NEMO project. Nucl. Instr. and Meth. A **630**, 107 (2011)

26. S. Viola et al., NEMO-SMO acoustic array: A deep-sea test of a novel acoustic positioning system for a km^3-scale underwater neutrino telescope. Nucl. Instr. and Meth. A **725**, 207 (2013)

27. S. Viola et al., Underwater acoustic positioning system for the SMO and KM3NeT-Italia projects. AIP Conference Proceedings **1630**, 134 (2014)

28. M. Circella for the NEMO collaboration, Time calibration of the NEutrino Mediterranean Observatory (NEMO). Nucl. Instr. and Meth. A **602**, 187 (2009)

29. S. Aiello et al., Measurement of the atmospheric muon depth intensity relation with the NEMO Phase-2 tower. Astropart. Phys. **66**, 1 (2015)

30. C. Hugon for the ANTARES and KM3NeT collaborations, Step by step simulation of phototubes for the KM3NeT and ANTARES optical modules. Nucl. Instr. and Meth. A **787**, 189 (2015)